Bioconjugate Chemistry

Article

pubs.acs.org/bc

Fluorescent Carbonaceous Nanodots for Noninvasive Glioma Imaging after Angiopep-2 Decoration

Shaobo Ruan,[†] Jun Qian,[‡] Shun Shen,[‡] Jiantao Chen,[†] Jianhua Zhu,[‡] Xinguo Jiang,[‡] Qin He,*[,†] Wuli Yang,*[,§] and Huile Gao*[,†]

[†]Key Laboratory of Drug Targeting and Drug Delivery Systems, West China School of Pharmacy, Sichuan University, No. 17, Block 3, Southern Renmin Road, Chengdu, 610041, China

[‡]Key Laboratory of Smart Drug Delivery (Fudan University), Ministry of Education; School of Pharmacy, Fudan University; 826 Zhangheng Road, Shanghai, 201203, China

[§]Department of Macromolecular Science & State Key Laboratory of Molecular Engineering of Polymers, Fudan University, Shanghai 200433, China

S *Supporting Information*

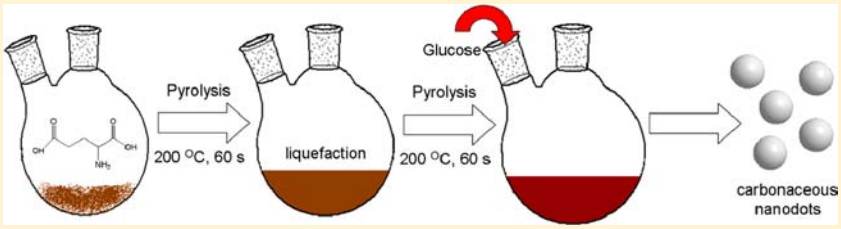

ABSTRACT: Fluorescent carbonaceous nanodots (CDs) have attracted much attention due to their unique properties. However, their application in noninvasive imaging of diseased tissues was restricted by the short excitation/emission wavelengths and the low diseased tissue accumulation efficiency. In this study, CDs were prepared from glucose and glutamic acid with a particle size of 4 nm. Obvious emission could be observed at 600 to 700 nm when CDs were excited at around 500 nm. This property enabled CDs with capacity for deep tissue imaging with low background adsorption. Angiopep-2, a ligand which could target glioma cells, was anchored onto CDs after PEGylation. The product, An-PEG-CDs, could target C6 glioma cells with higher intensity than PEGylated CDs (PEG-CDs), and endosomes were involved in the uptake process. In vivo, An-PEG-CDs could accumulate in the glioma site at higher intensity, as the glioma/normal brain ratio for An-PEG-CDs was 1.73. The targeting effect of An-PEG-CDs was further demonstrated by receptor staining, which showed An-PEG-CDs colocalized well with the receptors expressed in glioma. In conclusion, An-PEG-CDs could be successfully used for noninvasive glioma imaging.

INTRODUCTION

Fluorescent carbonaceous nanodots (CDs) have gained extensive attention due to not only their unique characteristics, such as green synthetic route, optical stability, good compatibility, and low toxicity, but also their great potential for application in detection and catalysis.[1−4] To obtain CDs, many methods have been developed, including thermal/hydrothermal oxidation, electrochemical synthesis, and microwave/ultrasonic synthesis.[2] Among which, one-step hydrothermal/thermal treatment methods have been widely used in producing CDs from various raw biomaterials, such as silk, juice, glucose, or other synthetic polymers.[5−7] However, most of these CDs showed short excitation/emission wavelengths (lower than 500 nm for excitation wavelength and 600 nm for emission wavelength), which restricted the application in bioimaging of diseases such as tumors, especially in the noninvasive whole body imaging, owing to the high background adsorption.[8−11] Thus, preparing CDs with long excitation/emission wavelengths was critical for expanding the application of CDs to noninvasive whole-body imaging. Unfortunately, few CDs displayed strong emission intensity when changing the excitation wavelength from blue or green to red or near-infrared region, and few studies have reported noninvasive whole body imaging of diseased tissue using these CDs.[1,12,13]

Besides the property of CDs, the physical barrier of the diseased tissue was another obstacle that restricted the application in noninvasive imaging. Brain tumors are an increasing threat for human beings. Gliomas account for 80% of original brain tumors.[14] Although surgery resection followed by chemotherapy/radiotherapy is still the standard procedure for glioma treatment, the survival time can only be expanded from 8 months to 15 months.[15] The poor survival time could be ascribed to both infiltration growth of glioma cells, which made it impossible to completely remove the glioma cells, and the blood brain barrier (BBB), which further restricted the access of chemotherapeutics by glioma cells.[16] Therefore, exact

Received: October 15, 2014
Revised: November 1, 2014
Published: November 11, 2014

   dx.doi.org/10.1021/bc500474p | *Bioconjugate Chem.* 2014, 25, 2252−2259

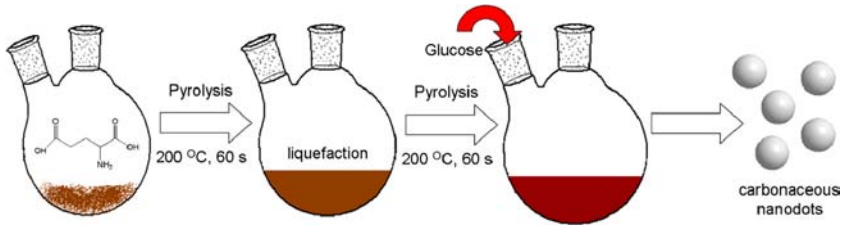

Figure 1. Elucidation of preparation procedure.

imaging of gliomas holds great perspective in helping surgeries to completely remove glioma cells, which may further expand the life span of glioma bearing patients. Presently, fluorescent imaging-aided surgical resection of tumor has been applied in the removal of peripheral tumors.[17] However, due to poor BBB penetration and glioma targeting capacity, most imaging probes cannot be applied in glioma imaging.[16] To conquer this barrier, ligand modification was usually used because the ligands could recognize specific receptors/carriers which are overexpressed on BBB and/or glioma cells.[16] Angiopep-2 is one such ligand whose receptor is low density lipoprotein receptor-related protein-1 (LRP1) that is overexpressed on both BBB and glioma cells, meaning that angiopep-2 could be used as an ideal ligand for glioma targeting.[18]

In this study, the fluorescent probe, CDs, was prepared by the simultaneous use of nontoxic glutamic acid and glucose (Figure 1). The fluorescent property enabled CDs with capacity for deep tissue imaging with low background adsorption. Angiopep-2 was anchored onto CDs after PEGylation, and the potential in glioma imaging was evaluated.

RESULTS AND DISCUSSION

Synthesis and Characterization. The hydrated particle size of CDs was 30.2 nm with a polydispersity index of 0.147, while the zeta potential was −23.5 mV. According to transmission electron microscopy (TEM) (Figure 2A and B), the particles were well dispersed with size around 4 nm (Figure 2C), and then the CDs were characterized by Fourier transform infrared spectroscopy (FTIR) (Figure 2D). The following vibrations were observed: stretching vibrations of C−OH at 3430 cm^{-1}, asymmetric stretching vibrations of C−NH−C at 1107 cm^{-1}, stretching vibrations of C═C at 1621 and 1512 cm^{-1}, stretching vibrations of $-CH_3$ and $-CH_2$ at 2900−2800 cm^{-1}, stretching vibrations of −C−O at 1326 cm^{-1}, indicating the structures of CDs might contain polycyclic aromatic and aromatic CN groups.[13,19,20] Surface states of the CDs were further characterized by X-ray photoelectron spectroscopy (XPS). The XPS spectrum showed three peaks at 288.7, 403.7, and 535.0 eV (Figure 2E), contributed by C_{1s}, N_{1s}, and O_{1s}, respectively. The C_{1s} spectrum (Supporting Information Figure S1A) showed four peaks at 287.7, 288.9, 290.1, and 291.3 eV, which were attributed to C−C, C−N, C−O, and C═N/C═O, respectively.[21] The N_{1s} spectrum (Supporting Information Figure S1B) exhibited three peaks at 402.5, 403.7, and 404.9 eV, which were contributed by the C−N−C, N−C, and N−H bands, respectively.[22] The O_{1s} spectrum (Supporting Information Figure S1C) displayed two peaks at 534.7 and 535.8 eV, which were attributed to C−OH/C−O−C and C═O groups, respectively.[20] These results demonstrated that the surface of CDs possessed plentiful oxygen and nitrogen functional groups, which was consistent with previous studies and useful for further modification.[20,21]

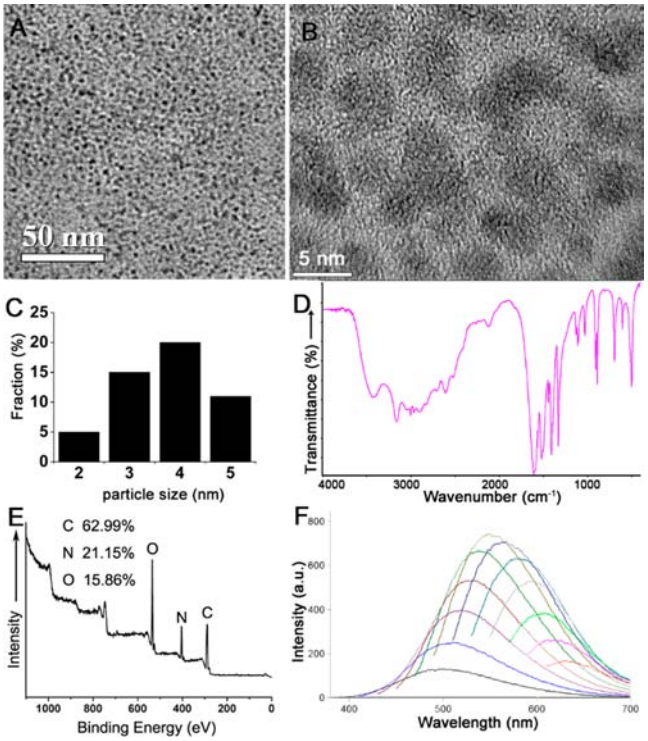

Figure 2. (A) TEM image of CDs. (B) High resolution of TEM image of CDs. (C) Particle size distribution of CDs. (D) FTIR spectrum of CDs. (E) XPS spectrum of CDs. (F) Fluorescent spectrum of CDs. The excitation wavelengths ranged from 340 to 560 nm with a step of 20 nm.

Interestingly, when we increased the excitation wavelength of the CDs from 340 to 440 nm, both the emission wavelengths and fluorescent intensity increased (Figure 2F), which was significantly different from previously reported CDs.[7,20] The highest emission wavelength was 552 nm while the excitation wavelength was 440 nm, which was longer than recently reported CDs possessing highest excitation/emission wavelength of 420 and 520 nm.[12] Additionally, further increasing the excitation wavelength could also expand the emission wavelength, displaying a broad excitation and emission range. Although the intensity peak of emission decreased with increasing excitation wavelengths from 440 to 560 nm, there were apparently still emission peaks. The quantum yield of CDs was 37.5%, which was higher than that of previously reported CDs.[9,23] Addtionally, CDs possessed better optical stability than traditional dyes.[24] The fluorescent property of the CDs was useful for in vivo imaging because longer excitation/emission wavelength could endow the CDs with the ability to penetrate deeper into tissues.

After PEGylation (PEG-CDs) and angiopep-2 modification (An-PEG-CDs), the hydrated particle sizes were changed to 35

dx.doi.org/10.1021/bc500474p | Bioconjugate Chem. 2014, 25, 2252−2259

and 38 nm (Supporting Information Table S1). The elevation in particle sizes was contributed by the surface modification. However, the zeta potential was not considerably changed. Compared with other carbon-based nanomaterials, such as carbon nanotubes and graphenes, CDs were spherical, leaving the modified PEG and ligands uniformly distributed on the surface, which was useful for escaping the reticuloendothelial system and being recognized by specific cells.[25,26]

Stability and Safety. In order to be used in biosystems, the serum stability and safety need to be addressed. First, serum stability was performed with incubation with different concentrations of serum for different periods of time (Figure 3). The serum stability significantly increased after PEGylation compared to bare CDs, owing to the PEGylation that could inhibit the adsorption of serum protein. An-PEG-CDs showed similar stability compared with PEG-CDs, indicating that angiopep-2 modification did not affect the serum stability.

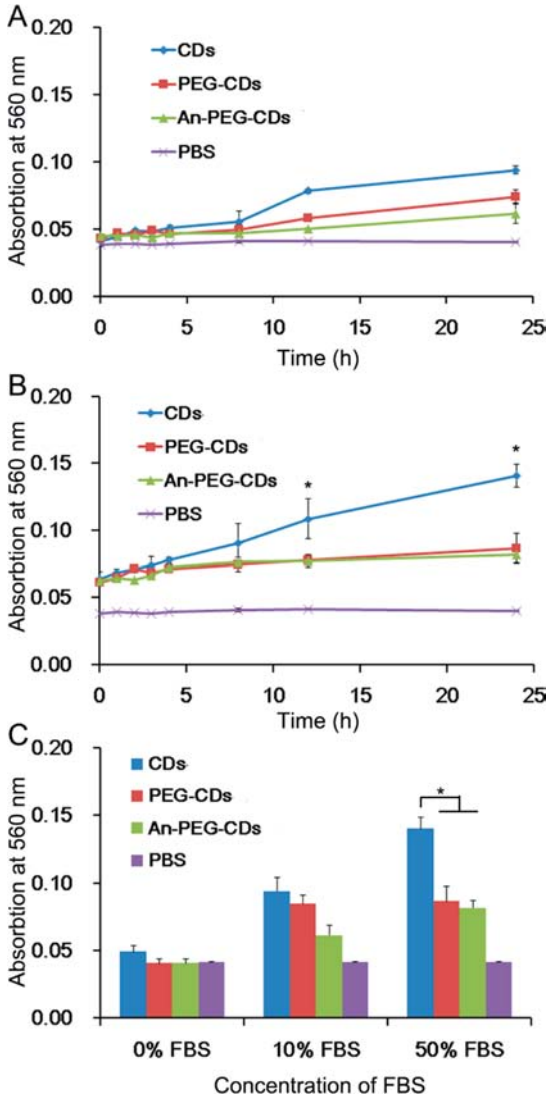

Figure 3. Serum stability of CDs, PEG-CDs, and An-PEG-CDs. (A) Time-related stability of 100 μg/mL of CDs, PEG-CDs, and An-PEG-CDs incubated with 10% FBS. (B) Time-related stability of 100 μg/mL of CDs, PEG-CDs, and An-PEG-CDs incubated with 50% FBS. *p < 0.05 vs PEG-CDs and An-PEG-CDs. (C) Stability of 100 μg/mL of CDs, PEG-CDs, and An-PEG-CDs incubated with different concentrations of FBS for 12 h. *p < 0.05.

The stability of CDs in PBS with different pH values was also carried out, which showed the CDs were stable in 8 h (Supporting Information Figure S2). However, further extending the incubation time could lead to obvious aggregation.

Second, hemocompatibility was carried out using fresh 2% blood red cells (Figure 4). Although the hemolysis rate

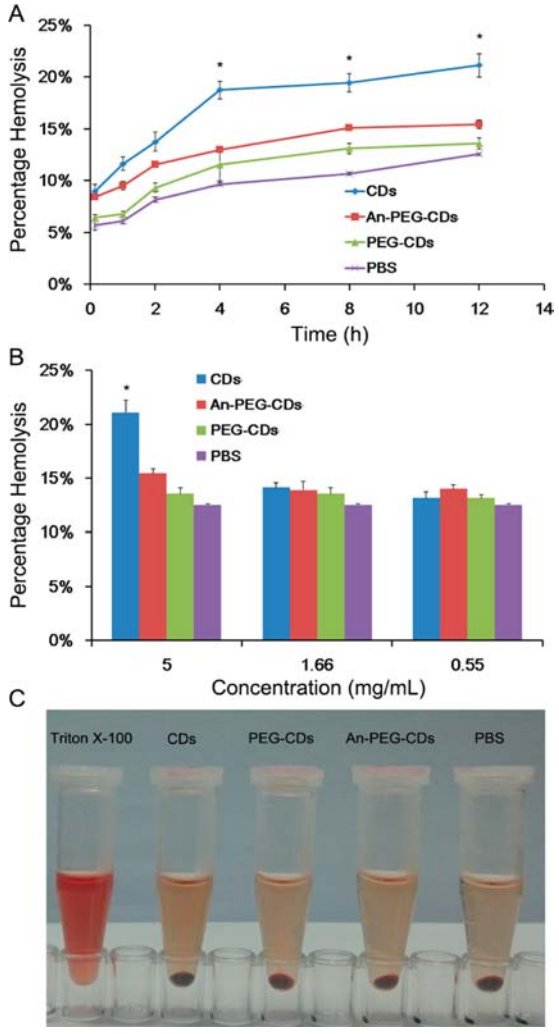

Figure 4. Hemocompatibility of CDs, PEG-CDs, and An-PEG-CDs. Time-related hemolysis rates of 5 mg/mL of CDs, PEG-CDs, and An-PEG-CDs. *p < 0.05 vs PEG-CDs and An-PEG-CDs. (B) Concentration related hemolysis rates of different concentrations of CDs, PEG-CDs, and An-PEG-CDs incubated with red blood cells for 8 h. *p < 0.05 vs PBS. (C) Image of red blood cells incubated with 5 mg/mL of CDs, PEG-CDs, and An-PEG-CDs for 8 h.

increased over time, the rates of PEG-CDs and An-PEG-CDs were significantly lower than that of CDs, indicating the PEGylation could improve the compatibility. After 12 h incubation, the hemolysis rates of PEG-CDs and An-PEG-CDs were approximately 14%, which was almost the same compared to PBS, suggesting that PEG-CDs and An-PEG-CDs could not obviously induce hemolysis.

Finally, MTT assay was performed on both C6 glioma cells and bEnd.3 cells (Figure 5). The cell viabilities of both C6 cells and bEnd.3 cells did not significantly decrease after 24 h incubation with CDs, PEG-CDs, or An-PEG-CDs at concentrations lower than 1 mg/mL. Although at higher concen-

dx.doi.org/10.1021/bc500474p | Bioconjugate Chem. 2014, 25, 2252−2259

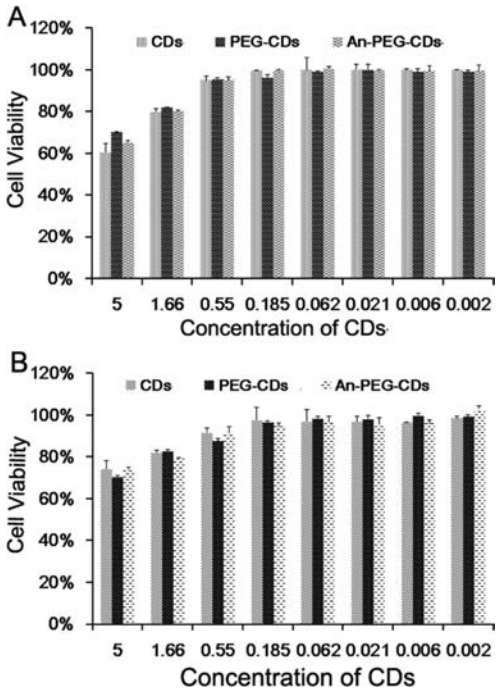

Figure 5. MTT assay of different concentrations of CDs, PEG-CDs, and An-PEG-CDs on C6 cells (A) and bEnd.3 cells (B).

trations, for example, 5 mg/mL, the cell proliferation could be considerably inhibited, the concentrations were much higher than those used for in vitro and in vivo imaging. Comparatively, 2.4 $\mu g/cm^2$ of carbon nanotubes could significantly inhibit the growth of cells,[27] while 150 nM of CdTe dots could significantly inhibit the cell growth.[28] Thus, it could be concluded that CDs, PEG-CDs, and An-PEG-CDs displayed low cytotoxicity.

Cellular Response Assay. To determine their potentiality in glioma imaging, in vitro cellular uptake was carried out. The uptake of PEG-CDs by C6 glioma cells was concentration- and time-dependent (Figure 6A,B), which was consistent with other particles.[9,29] Angiopep-2 modification could apparently increase the cellular uptake, owing to the highly expressed LRP1 on C6 cells,[30] which was the specific receptor of angiopep-2. Normally, receptor-mediated cellular uptake of particles was internalized through endosomes.[31] Thus, the endosomes colocalization assay was performed. It showed relatively high colocalization of An-PEG-CDs with endosomes after 1 h incubation, while the colocalization was considerably decreased after 4 h incubation and most of An-PEG-CDs were located in cytoplasm rather than endosomes, suggesting that enhanced cellular uptake of An-PEG-CDs was mediated by endosomes, which was consistent with other ligand modified nanoparticles.[32] These results demonstrated that An-PEG-CDs could target to C6 glioma cells, indicating they might be used for glioma imaging. Additionally, the internalization of both unmodified and ligand modified nanoparticles involved endosomes, although they may be through different pathways.[33,34] For example, ligand modified nanoparticles were mainly internalized through clathrin-mediated pathways while unmodified nanoparticles might be through macropinocytosis.[35]

In Vivo Imaging. After i.v. injected into mice through tail vein at a dose of 50 mg/kg, both PEG-CDs and An-PEG-CDs could distribute into the brain site, while the intensity of mice injected with An-PEG-CDs was much higher than that of PEG-

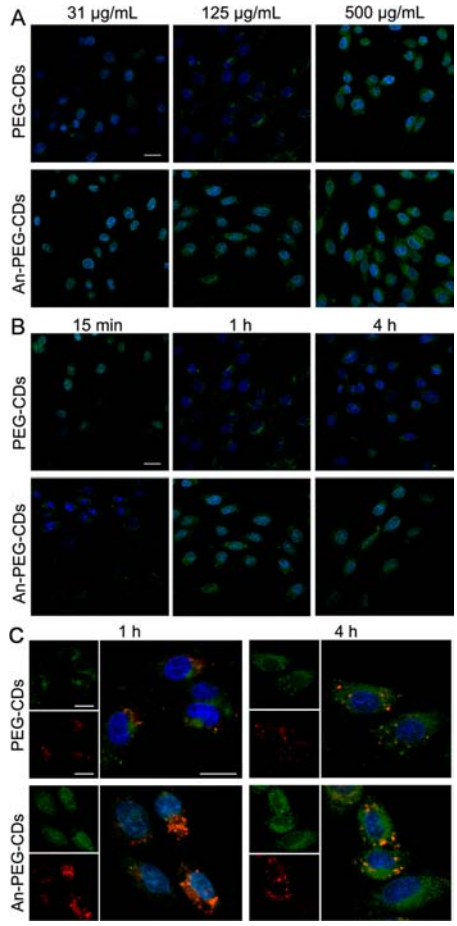

Figure 6. C6 cellular response of PEG-CDs and An-PEG-CDs. (A) different concentrations of PEG-CDs and An-PEG-CDs incubated with C6 cells for 1 h. (B) 125 $\mu g/mL$ of PEG-CDs and An-PEG-CDs incubated with C6 cells for different period of time. (C) Colocalization of particles with endosomes after C6 cells incubated with 125 $\mu g/mL$ of PEG-CDs and An-PEG-CDs for 1 or 4 h. Bar represents 10 μm.

CDs group (Supporting Information Figure S3), suggesting that modification of angiopep-2 could improve the glioma targeting effect of PEG-CDs, which was consistent with other angiopep-2 modified nanoparticles.[18] The fluorescent intensities in the brain site achieved their highest peaks at 30 min after injection and then the intensities decreased gradually. At 2 h after injection, three-dimensional (3D) reconstruction was performed (Figure 7A). The fluorescence of both groups was focused on the glioma site, while the intensity of An-PEG-CDs group was approximately 2-fold higher than that of PEG-CDs group. Ex vivo imaging could more directly reflect the targeting effect of An-PEG-CDs. The fluorescent intensity in the normal brain (right part) was almost the same for both An-PEG-CDs group and PEG-CDs group (Figure 7B,C). However, the intensity in the glioma site of An-PEG-CDs group was much higher than that of PEG-CDs groups, which was approximately 1.56-fold as the latter. To directly compare the glioma targeting efficiency of PEG-CDs and An-PEG-CDs, the glioma/normal brain ratio (G/N ratio) was calculated (Figure 7D). The G/N ratio for PEG-CDs group is 1.12, indicating a slight glioma targeting ability, which was mainly due to the EPR effect.[36] However, the ratio for the An-PEG-CDs group is as high as 1.73, suggesting obvious glioma targeting efficiency which contributed to the angiopep-2 modification. Additionally, there

dx.doi.org/10.1021/bc500474p | Bioconjugate Chem. 2014, 25, 2252−2259

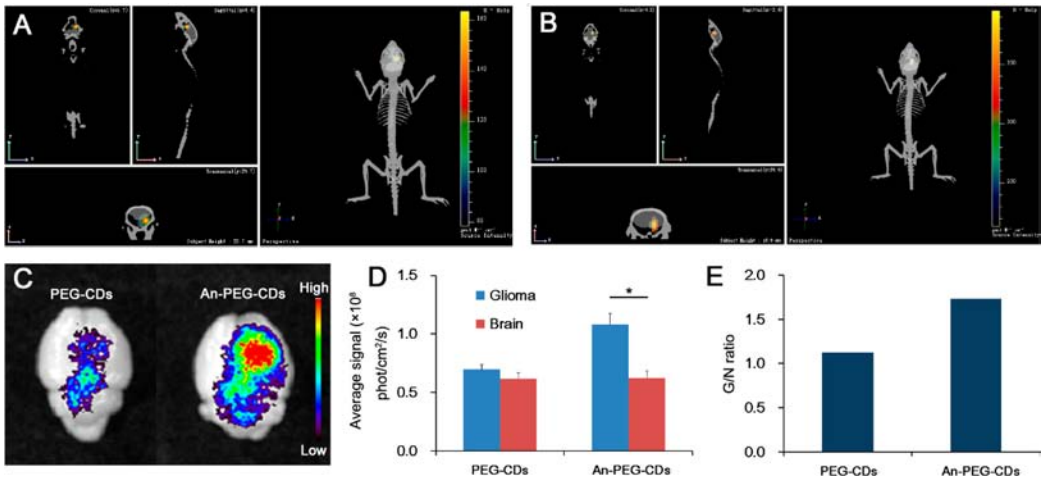

Figure 7. In vivo and ex vivo imaging at 2 h after injection. (A) 3D reconstruction of in vivo imaging of PEG-CDs treated mice. (B) 3D reconstruction of in vivo imaging of An-PEG-CDs treated mice. (C) Ex vivo imaging of glioma bearing brain. (D) Semiquantitative fluorescent intensity of brain and glioma. $*p < 0.05$. (E) G/N ratio of PEG-CDs and An-PEG-CDs group.

was no obvious difference between PEG-CDs and An-PEG-CDs in the distribution in normal tissues (Supporting Information Figure S4), indicating that angiopep-2 modification did not elevate the distribution of particles in normal tissues.

To further evaluate the glioma distribution of PEG-CDs and An-PEG-CDs, tissue slices were prepared and stained with anti-LRP1 antibody (Figure 8). Glioma cells could be stained into

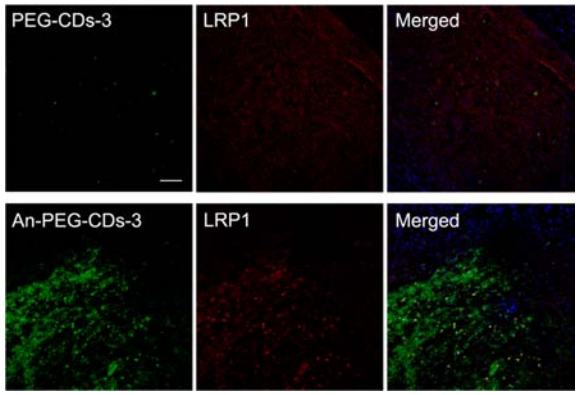

Figure 8. Distribution of PEG-CDs and An-PEG-CDs in brain slices. LRP1 was stained by anti-LRP1 antibody. Bar represents 100 μm.

red by anti-LRP1 antibody. It showed that only a small amount of PEG-CDs were distributed in LRP1 positive glioma cells. In contrast, a much higher intensity of An-PEG-CDs could be observed in glioma cells and they well colocalized with glioma cells. Besides, the distribution of PEG-CDs and An-PEG-CDs in slices of normal tissues showed no significant difference (Supporting Information Figure S3), which was consistent with ex vivo imaging results. In combination with in vitro and in vivo experiments, the results strongly demonstrated that angiopep-2 modification could improve the glioma targeting efficiency of PEG-CDs, making An-PEG-CDs an effective noninvasive glioma imaging probe.

CONCLUSION

In this study, a kind of CD was prepared with long excitation/emission wavelength. After surface modification with PEG and angiopep-2, these CDs could be used for glioma imaging. In vitro, the C6 cellular uptake of An-PEG-CDs was higher than that of PEG-CDs, which was mediated by endosomes. In vivo, An-PEG-CDs showed significantly higher glioma targeting efficiency than PEG-CDs. The G/N ratio for An-PEG-CDs was 1.76, which was considerably higher than that of PEG-CDs. Additionally, An-PEG-CDs displayed good serum stability, hemocompatibility, and low cytotoxicity. These results demonstrated that An-PEG-CDs were excellent probes for glioma noninvasive imaging.

MATERIALS AND METHODS

Materials. Glutamic acid and glucose were purchased from Sinopharm Chemical Reagent (Shanghai, China). C6 cell line was purchased from the Institute of Biochemistry and Cell Biology, Shanghai Institutes for Biological Sciences, Chinese Academy of Sciences (Shanghai, China). The bEnd.3 cell line was purchased from American type culture collection (ATCC) (VA, USA). Dulbecco's Modified Eagle Medium (high glucose) cell culture medium (DMEM) and FBS were purchased from Life Technologies (NY, USA). Cell culturing dishes and plates were purchased from Wuxi NEST Biotechnology Co. Ltd. (Wuxi, China). *N*-(3-(Dimethylamino)propyl)-*N*′-ethylcarbodiimide hydrochloride (EDC), *N*-hydroxy-succinimide (NHS), and coumarin-6 were purchased from Sigma (MO, USA). DAPI was purchased from Beyotime (Haimen, China). Rabbit anti-LRP1 antibody was purchased from Abcam (Hong Kong, China). Alexafluor 594-conjugated donkey anti-rabbit antibody was purchased from Jackson Immunoresearch Laboratories, Inc. (PA, USA). LysoTracker red was purchased from Life Technologies (NY, USA).

BALB/c nude mice (male, 4−5 weeks, 18−22 g) were obtained from the Animal Research Center of Sichuan University (Chengdu, China) and maintained under standard housing conditions. All animal experiments were carried out in accordance with protocols evaluated and approved by the ethics committee of Sichuan University.

Synthesis and Characterization of An-PEG-CDs. A dry flask (100 mL) was heated to 200 °C, and then 1 g of glutamic acid was added. One minute later, 0.1 g of glucose was added and the heater was removed. When the temperature of the flask decreased to approximately 50 °C, 5 mL of deionized water was

dx.doi.org/10.1021/bc500474p | *Bioconjugate Chem.* 2014, 25, 2252−2259

added to suspend the produced CDs. The particle size and morphology were observed through transmission electron microscope (H-600, Hitachi, Japan). The hydrated particle size and zeta potential were determined by a zeta/particle sizer (Malvern, NanoZS, Germany). Fluorescence spectrum was evaluated using a RF-5301PC spectrofluorophotometer (Shimadzu, Japan). Fourier transform infrared (FTIR) spectra were determined on a Bruker Vector22 spectrometer (Germany) using spectroscopic grade KBr. X-ray photoelectron spectroscopy (XPS) experiments were performed on an AXIS Ultra DLD (Kratos UK) with Mg Ka radiation ($h\nu$ =1486.6 eV), with a chamber pressure of 2.2×10^{-9} Torr. The source power and high voltage were set at 150 W and 15 kV, and pass energies of 40 eV for survey scans were used. The analysis spot size was 300×700 μm^2. The data was analyzed by PHI-MATLAB software with C_{1s} = 284.6 eV as a benchmark for the binding energy correction.

To prepare PEG-CDs and An-PEG-CDs, angiopep-2 first reacted with MAL-PEG-COOH at pH 7.4 PBS for 12 h. Then, the product, angiopep-2 conjugated PEG (An-PEG-COOH), was harvested after dialysis (MW = 3400 D) and lyophilization. Then, PEG-COOH and An-PEG-COOH were activated by EDC/NHS for 0.5 h, followed by the addition of CDs. After 12 h incubation, the PEG-CDs and An-PEG-CDs could be obtained after dialysis (MW = 10 000 D).

Serum Stability and Safety. The stability of CDs was evaluated in PBS with different concentrations of FBS. CDs, PEG-CDs, and An-PEG-CDs were suspended in 0%, 10%, or 50% FBS and incubated in a 37 °C incubator. The absorption at 560 nm was determined by a microplate reader (Multiskan MK3, Thermo, USA) at 0, 1, 2, 3, 4, 6, 8, 12, and 24 h.

To evaluate the hemocompatibility, whole blood was collected from mice using heparin as anticoagulant. After centrifugation at 1500 rpm for 5 min, the red blood cells were resuspended in PBS at the final density of 2%. Different concentrations of CDs, PEG-CDs, and An-PEG-CDs were added into the cell suspension and incubated at 37 °C for different periods of time. After incubation, cell suspension was centrifuged at 1500 rpm for 5 min, and the adsorption of supernatant at 560 nm was determined by a microplate reader (Thermo Scientific Varioskan Flash, USA). 1% of Triton X-100 was used as positive control and PBS was used as negative control.

The cytotoxicity of different formulations was evaluated by MTT assay. C6 cells and bEnd.3 cells (2×10^4 cells/mL) were seeded in 96-well plates. Twenty-four hours later, CDs, PEG-CDs, and An-PEG-CDs were added into wells with serial concentrations ranging from 5 mg/mL to 1 μg/mL. Twenty-four hours later, 100 μL of MTT solution was added into each well and incubated for 4 h. After replacing the medium with DMSO, the 450 nm absorption was observed by a microplate reader (Thermo Scientific Varioskan Flash, USA).

In Vitro Cellular Uptake and Subcellular Localization. C6 cells were seeded in 6 cm glass-bottom dishes at a density of 1×10^4 cells/mL and incubated at 37 °C for 24 h.[37,38] After 5 min incubation in PBS, the cells were treated with different concentrations of PEG-CDs and An-PEG-CDs for different times. After incubation, the cells were washed, fixed, and stained with 0.5 μg/mL of DAPI. Images were captured with a confocal microscope (LSM710, Carl Zeiss, Germany).

To determine the subcellular colocalization with endosomes, C6 cells were seeded into dishes as described above and incubated with 125 μg/mL of CD for 0.25 or 4 h. Thirty minutes before the incubation ended, Lysotracker Red (100 nmol/L) was added into the wells. After incubation, the cells were washed, fixed, and stained with 0.5 μg/mL of DAPI. Images were captured with a confocal microscope (LSM710, Carl Zeiss, Germany).

In Vivo and Ex Vivo Imaging and Slice Distribution. The orthotopic C6 glioma bearing mice were established as described previously.[39,40] Nude mice was anesthetized and placed onto a stereotaxic apparatus. Five microliters of PBS containing 5×10^5 C6 cells was slowly injected into the right brain of mice (1.8 mm lateral to bregma). Twelve days later, mice were i.v. administered 50 mg/kg of PEG-CDs or An-PEG-CDs through the tail vein. Then the whole body fluorescent distribution was observed through an in vivo imaging system using excitation/emission wavelength of 500/600 nm (IVIS Spectrum, Caliper, USA) 5, 15, 30, 60, and 120 min after injection, and a 3D fluorescent distribution in brain was observed. Then, the mice were sacrificed, and their tissues were subjected to ex vivo fluorescence imaging. After fixing with 4% paraformaldehyde, organs were further dehydrated by 15% sucrose followed with 30% sucrose. Consecutive frozen sections of 10 μm thicknesses were prepared and then stained by 0.5 μg/mL DAPI for 5 min. For brain slices, LRP1 was stained with rabbit anti-LRP1 antibody (1:200) followed with Alexafluor 594 conjugated donkey anti-rabbit antibody according to previous established procedure.[41] The distribution of fluorescence was observed by a confocal microscope (LSM710, Carl Zeiss, Germany).

Statistical Analysis. Statistical differences were evaluated with Student's t test. p-Values less than 0.05 were considered to be statistically significant.

■ ASSOCIATED CONTENT

Ⓢ Supporting Information

Particle size and zeta potential of PEG-CDs and An-PEG-CDs; XPS spectrum; Stability of CDs in PBS with different pH; In vivo and ex vivo imaging; Distribution of PEG-CDs and An-PEG-CDs in normal tissue slices. This material is available free of charge via the Internet at http://pubs.acs.org.

■ AUTHOR INFORMATION

Corresponding Authors

*E-mail: qinhe@scu.edu.cn.
*E-mail: wlyang@fudan.edu.cn.
*E-mail: gaohuile@scu.edu.cn. Fax: 86 28 85502532. Tel: 86 28 85502575.

Author Contributions

Shaobo Ruan and Jun Qian contributed equally to this work.

Notes

The authors declare no competing financial interest.

■ ACKNOWLEDGMENTS

The work was granted by the National Basic Research Program of China (973 Program, 2013CB932504), National Natural Science Foundation of China (81402866, 81373337) and the Sichuan University Starting Foundation for Young Teachers (2014SCU11044).

■ REFERENCES

(1) Du, F., Ming, Y., Zeng, F., Yu, C., and Wu, S. (2013) A low cytotoxic and ratiometric fluorescent nanosensor based on carbon-dots for intracellular pH sensing and mapping. *Nanotechnology 24*, 365101.

(2) Li, H., Kang, Z., Liu, Y., and Lee, S. (2012) Carbon nanodots: synthesis, properties and applications. *J. Mater. Chem. 22*, 24230−24253.
(3) Baker, S. N., and Baker, G. A. (2010) Luminescent carbon nanodots: emergent nanolights. *Angew. Chem., Int. Ed. 49*, 6726−44.
(4) Cao, L., Wang, X., Meziani, M. J., Lu, F., Wang, H., Luo, P. G., Lin, Y., Harruff, B. A., Veca, L. M., Murray, D., Xie, S. Y., and Sun, Y. P. (2007) Carbon dots for multiphoton bioimaging. *J. Am. Chem. Soc. 129*, 11318−9.
(5) Chen, B., Li, F., Li, S., Weng, W., Guo, H., Guo, T., Zhang, X., Chen, Y., Huang, T., Hong, X., You, S., Lin, Y., Zeng, K., and Chen, S. (2013) Large scale synthesis of photoluminescent carbon nanodots and their application for bioimaging. *Nanoscale 5*, 1967−71.
(6) Sahu, S., Behera, B., Maiti, T. K., and Mohapatra, S. (2012) Simple one-step synthesis of highly luminescent carbon dots from orange juice: application as excellent bio-imaging agents. *Chem. Commun. (Cambridge) 48*, 8835−7.
(7) Liu, S., Tian, J., Wang, L., Luo, Y., Zhai, J., and Sun, X. (2011) Preparation of photoluminescent carbon nitride dots from CCl4 and 1,2-ethylenediamine: a heat-treatment-based strategy. *J. Mater. Chem. 21*, 11726−11729.
(8) Bhunia, S. K., Saha, A., Maity, A. R., Ray, S. C., and Jana, N. R. (2013) Carbon nanoparticle-based fluorescent bioimaging probes. *Sci. Rep. 3*, 1473.
(9) Ruan, S., Zhu, B., Zhang, H., Chen, J., Shen, S., Qian, J., He, Q., and Gao, H. (2014) A simple one-step method for preparation of fluorescent carbon nanospheres and the potential application in cell organelles imaging. *J. Colloid Interface Sci. 422*, 25−9.
(10) Schroeder, B. R., Ghare, M. I., Bhattacharya, C., Paul, R., Yu, Z., Zaleski, P. A., Bozeman, T. C., Rishel, M. J., and Hecht, S. M. (2014) The disaccharide moiety of bleomycin facilitates uptake by cancer cells. *J. Am. Chem. Soc. 136*, 13641−56.
(11) Bhattacharya, C., Yu, Z., Rishel, M. J., and Hecht, S. M. (2014) The carbamoylmannose moiety of bleomycin mediates selective tumor cell targeting. *Biochemistry 53*, 3264−6.
(12) Ko, H. Y., Chang, Y. W., Paramasivam, G., Jeong, M. S., Cho, S., and Kim, S. (2013) In vivo imaging of tumour bearing near-infrared fluorescence-emitting carbon nanodots derived from tire soot. *Chem. Commun. (Cambridge) 49*, 10290−2.
(13) Zhu, S., Meng, Q., Wang, L., Zhang, J., Song, Y., Jin, H., Zhang, K., Sun, H., Wang, H., and Yang, B. (2013) Highly photoluminescent carbon dots for multicolor patterning, sensors, and bioimaging. *Angew. Chem., Int. Ed. 52*, 3953−7.
(14) Agarwal, S., Sane, R., Oberoi, R., Ohlfest, J. R., and Elmquist, W. F. (2011) Delivery of molecularly targeted therapy to malignant glioma, a disease of the whole brain. *Expert Rev. Mol. Med. 13*, e17.
(15) Clarke, J., Butowski, N., and Chang, S. (2010) Recent advances in therapy for glioblastoma. *Arch. Neurol. 67*, 279−83.
(16) Gao, H., Pang, Z., and Jiang, X. (2013) Targeted delivery of nano-therapeutics for major disorders of the central nervous system. *Pharm. Res. 30*, 2485−98.
(17) Nguyen, Q. T., Olson, E. S., Aguilera, T. A., Jiang, T., Scadeng, M., Ellies, L. G., and Tsien, R. Y. (2010) Surgery with molecular fluorescence imaging using activatable cell-penetrating peptides decreases residual cancer and improves survival. *Proc. Natl. Acad. Sci. U. S. A. 107*, 4317−22.
(18) Xin, H., Jiang, X., Gu, J., Sha, X., Chen, L., Law, K., Chen, Y., Wang, X., Jiang, Y., and Fang, X. (2011) Angiopep-conjugated poly(ethylene glycol)-co-poly(epsilon-caprolactone) nanoparticles as dual-targeting drug delivery system for brain glioma. *Biomaterials 32*, 4293−305.
(19) Pan, D., Zhang, J., Li, Z., Wu, C., Yan, X., and Wu, M. (2010) Observation of pH-, solvent-, spin-, and excitation-dependent blue photoluminescence from carbon nanoparticles. *Chem. Commun. (Cambridge) 46*, 3681−3.
(20) Li, W., Zhang, Z., Kong, B., Feng, S., Wang, J., Wang, L., Yang, J., Zhang, F., Wu, P., and Zhao, D. (2013) Simple and green synthesis of nitrogen-doped photoluminescent carbonaceous nanospheres for bioimaging. *Angew. Chem., Int. Ed. 52*, 8151−5.
(21) Sevilla, M., and Fuertes, A. B. (2009) Chemical and structural properties of carbonaceous products obtained by hydrothermal carbonization of saccharides. *Chem.—Eur. J. 15*, 4195−4203.
(22) Liu, S., Tian, J., Wang, L., Zhang, Y., Qin, X., Luo, Y., Asiri, A. M., Al-Youbi, A. O., and Sun, X. (2012) Hydrothermal treatment of grass: a low-cost, green route to nitrogen-doped, carbon-rich, photoluminescent polymer nanodots as an effective fluorescent sensing platform for label-free detection of Cu(II) ions. *Adv. Mater. 24*, 2037−2041.
(23) Ruan, S., Qian, J., Shen, S., Zhu, J., Jiang, X., He, Q., and Gao, H. (2014) A simple one-step method to prepare fluorescent carbon dots and their potential application in non-invasive glioma imaging. *Nanoscale 6*, 10040−10047.
(24) Cao, L., Meziani, M. J., Sahu, S., and Sun, Y. P. (2013) Photoluminescence properties of graphene versus other carbon nanomaterials. *Acc. Chem. Res. 46*, 171−80.
(25) Campbell, A. S., Dong, C., Meng, F., Hardinger, J., Perhinschi, G., Wu, N., and Dinu, C. Z. (2014) Enzyme catalytic efficiency: a function of bio-nano interface reactions. *ACS Appl. Mater. Interfaces 6*, 5393−403.
(26) Casals, E., and Puntes, V. F. (2012) Inorganic nanoparticle biomolecular corona: formation, evolution and biological impact. *Nanomedicine (London) 7*, 1917−30.
(27) Siegrist, K. J., Reynolds, S. H., Kashon, M. L., Lowry, D. T., Dong, C., Hubbs, A. F., Young, S. H., Salisbury, J. L., Porter, D. W., Benkovic, S. A., McCawley, M., Keane, M. J., Mastovich, J. T., Bunker, K. L., Cena, L. G., Sparrow, M. C., Sturgeon, J. L., Dinu, C. Z., and Sargent, L. M. (2014) Genotoxicity of multi-walled carbon nanotubes at occupationally relevant doses. *Part. Fibre Toxicol. 11*, 6.
(28) Chen, N., He, Y., Su, Y., Li, X., Huang, Q., Wang, H., Zhang, X., Tai, R., and Fan, C. (2012) The cytotoxicity of cadmium-based quantum dots. *Biomaterials 33*, 1238−44.
(29) Gao, H., Hu, G., Zhang, Q., Zhang, S., Jiang, X., and He, Q. (2014) Pretreatment with chemotherapeutics for enhanced nanoparticles accumulation in tumor: the potential role of G2 cycle retention effect. *Sci. Rep. 4*, 4492.
(30) Maletinska, L., Blakely, E. A., Bjornstad, K. A., Deen, D. F., Knoff, L. J., and Forte, T. M. (2000) Human glioblastoma cell lines: levels of low-density lipoprotein receptor and low-density lipoprotein receptor-related protein. *Cancer Res. 60*, 2300−3.
(31) Mahmoudi, M., Azadmanesh, K., Shokrgozar, M. A., Journeay, W. S., and Laurent, S. (2011) Effect of nanoparticles on the cell life cycle. *Chem. Rev. 111*, 3407−32.
(32) Gao, H., Yang, Z., Zhang, S., Pang, Z., Liu, Q., and Jiang, X. (2014) Study and evaluation of mechanisms of dual targeting drug delivery system with tumor microenvironment assays compared with normal assays. *Acta Biomater. 10*, 858−67.
(33) Liu, Y., Ji, M., Wong, M. K., Joo, K. I., and Wang, P. (2013) Enhanced therapeutic efficacy of iRGD-conjugated crosslinked multilayer liposomes for drug delivery. *Biomed. Res. Int. 2013*, 378380.
(34) Joo, K. I., Xiao, L., Liu, S., Liu, Y., Lee, C. L., Conti, P. S., Wong, M. K., Li, Z., and Wang, P. (2013) Crosslinked multilamellar liposomes for controlled delivery of anticancer drugs. *Biomaterials 34*, 3098−109.
(35) Gao, H., Yang, Z., Zhang, S., Cao, S., Shen, S., Pang, Z., and Jiang, X. (2013) Ligand modified nanoparticles increases cell uptake, alters endocytosis and elevates glioma distribution and internalization. *Sci. Rep. 3*, 2534.
(36) Liu, Y., and Lu, W. (2012) Recent advances in brain tumor-targeted nano-drug delivery systems. *Expert Opin. Drug Delivery 9*, 671−86.
(37) Wu, J., Yamanouchi, D., Liu, B., and Chu, C. C. (2012) Biodegradable arginine-based poly(ether ester amide)s as a non-viral DNA delivery vector and their structure-function study. *J. Mater. Chem. 22*, 18983−18991.
(38) Yu, Z., Schmaltz, R. M., Bozeman, T. C., Paul, R., Rishel, M. J., Tsosie, K. S., and Hecht, S. M. (2013) Selective tumor cell targeting by the disaccharide moiety of bleomycin. *J. Am. Chem. Soc. 135*, 2883−6.

(39) Gao, H., Qian, J., Yang, Z., Pang, Z., Xi, Z., Cao, S., Wang, Y., Pan, S., Zhang, S., Wang, W., Jiang, X., and Zhang, Q. (2012) Whole-cell SELEX aptamer-functionalised poly(ethyleneglycol)-poly(epsilon-caprolactone) nanoparticles for enhanced targeted glioblastoma therapy. *Biomaterials 33*, 6264−72.
(40) Gao, H., Pang, Z., Pan, S., Cao, S., Yang, Z., Chen, C., and Jiang, X. (2012) Anti-glioma effect and safety of docetaxel-loaded nano-emulsion. *Arch. Pharm. Res. 35*, 333−41.
(41) Gao, H., Pan, S., Yang, Z., Cao, S., Chen, C., Jiang, X., Shen, S., Pang, Z., and Hu, Y. (2011) A cascade targeting strategy for brain neuroglial cells employing nanoparticles modified with angiopep-2 peptide and EGFP-EGF1 protein. *Biomaterials 32*, 8669−8675.